Available online at www.sciencedirect.com
SCIENCE DIRECT
Remote Sensing of Environment 95 (2005) 150–163
Remote Sensing of Environment
www.elsevier.com/locate/rse

ENVISAT radar altimeter measurements over continental surfaces and ice caps using the ICE-2 retracking algorithm

Benoit Legresy[a,*], Fabrice Papa[a], Frederique Remy[a], Gaetan Vinay[a], Mathias van den Bosch[b], Ouan-Zan Zanife[b]

[a]CNRS-CNES-UPS-IRD, LEGOS, 18 Avenue Edouard BELIN, 31401 Toulouse, France
[b]Collecte Localisation Satellite-CLS, Space Oceanography Division, 31480 Ramonville St. Agne, France

Received 17 May 2004; received in revised form 15 November 2004; accepted 28 November 2004

Abstract

This study presents the first results obtained with the ENVISAT satellite radar altimeter RA-2 over lands and ice caps. As radar altimetry was firstly devoted to ocean study, this paper starts with a detailed description of the radar altimetry principle over continental surfaces: a general formulation of the radar altimeter echoes according to different surface types is given and the retracking procedure ICE-2, specially implemented on the ENVISAT satellite ground segment to provide output parameters over continents, is clearly presented. The ENVISAT RA-2 datasets processed with the ICE-2 procedure are then mapped given an overall description of the output parameters over various surfaces. The behaviour of these ENVISAT altimetric parameters are analysed and related to main land surface characteristics such as surface/volume echo, specularity, roughness.... Apart from few unexpected signals which will need to be further investigated, the new ENVISAT dataset confirms the potential of inland altimetry and provides a new opportunity to monitor continental surfaces. The Ku band measurements confirm previous results recently obtained with the altimeters on board ERS or Topex–Poseidon and offer a temporal continuity. The S band altimeter measurements are in accordance with theoretical expected ones and confirm previous Topex–Poseidon observations in C band. The S band and the use of the dual-frequency thus bring new capabilities for altimetric applications with important deliveries for temporal evolution survey. For instance, S band will be used over continents to better detect wetlands located under vegetated areas or to better quantify wave penetration in terrestrial snowpack to accurately retrieve snow depth evolution. Over ice sheets, the dual-frequency S and Ku band waveforms parameters will provide a more accurate height estimation as it will be possible to quantify the error on height measurements induced by snowpack structure change over time. This will then provide a more confident survey of the ice sheets surface topography evolution.

The combination and complementarities with the other altimetry missions such as ERS, Topex–Poseidon and Jason look already promising and offer a 10-year span dataset for continental altimetry applications.

Keywords: ENVISAT; Radar; Altimeter; Ice caps; Continental surfaces

1. Introduction

The satellite radar altimeters are nadir-pointing active microwave sensors initially developed to operate over ocean surfaces and make precise measurements of the sea surface topography (Fu & Cazenave, 2001). However, they rapidly exhibited on their strong capabilities to provide information over continental surfaces (Zwally et al., 1983). Up to recently, radar altimetry was mainly applied over ice caps in order to construct precise topography (Remy et al., 1990, 1999), to characterise the snow surface roughness and snowpack structure (Legresy & Remy, 1997, 1998; Remy et al., 1990, 1996) or to survey the temporal height variations (Zwally et al., 1989).

In parallel, the ability of radar altimeter to monitor inland water surfaces and measure their stage elevation has been

* Corresponding author. Tel.: +33 5 61 33 29 56; fax: +33 5 61 25 32 05.
E-mail address: benoit.legresy@cnes.fr (B. Legresy).

0034-4257/$ - see front matter © 2005 Elsevier Inc. All rights reserved.
doi:10.1016/j.rse.2004.11.018

also demonstrated over a wide variety of continental water bodies (Birkett, 1995; Cazenave et al., 1997). The extension of radar altimetry technique to survey lakes, rivers and flood plains level fluctuations makes this sensor a powerful tool to study regional hydrological systems (Alsdorf et al., 2001; Cazenave et al., 1997).

Recently, the use of the dual-frequency NRA radar altimeter on board the Topex–Poseidon satellite have demonstrated new capabilities over continental surfaces (Papa et al., 2002, 2003): the radar altimeter backscattering coefficient was successfully used to classify major global surface properties and to study their temporal evolution (Papa et al., 2003). For instance, radar altimetry was used over the Northern Great Plains to survey snow cover and determine the beginning and the end of the snow season and the evolution of the snow depths during the winter (Papa et al., 2002). Moreover, the altimeter backscatter analyses showed promising results over vegetated areas, deserts or wetlands to be further investigated.

However, in general, altimetric data collected over continents are usually processed and optimized for ocean surfaces which restrained their use for continental applications. With the introduction of radar altimetry applications over the ice sheets, a new retracking procedure was developed, the so called ICE-2 retracker. It has been designed to process altimeter waveforms obtained over most of the non-ocean surfaces. This technique was first applied with success to the ERS altimeter data (Legresy & Remy, 1997; Remy et al., 1999; Vinay et al., 2002). This processing has been now included directly in the ENVISAT radar altimeter ground segment, which enables retracked data to be delivered to the users for continental surface applications.

In that context, this paper intends to describe the principle of altimetry over land surfaces and the retracking procedure ICE-2 considering the first ENVISAT radar altimeter measurements. To this end, we mapped the ENVISAT datasets processed with the ICE-2 procedure and give a precise description of the output parameters obtained over land and ice caps. The behaviour of these parameters over the various surface types is clearly explained and offer real new potentials for inland altimetry applications. In particular the S band altimeter measurements are shown to bring improvements to study complex vegetated areas or snowpack structures.

2. Altimetric signal and retracking procedure

2.1. Basic theory of altimetric echoes

Over ocean-like surfaces, the altimeter echo can be seen as the sum of the reflections from elementary surface facets distributed around the mean surface ordered by their arrival time or range (Brown, 1977). The waveform shape (Fig. 1) results from the convolution of the impulse response shape

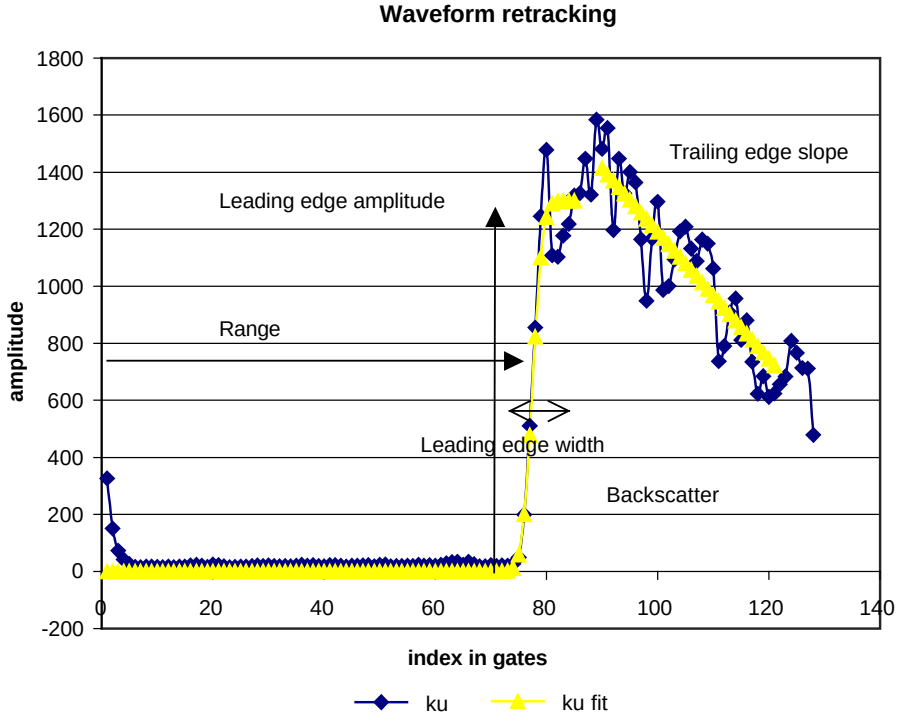

Fig. 1. The altimetric waveform is represented in blue and the fitting function from the retracking in yellow. The different parameters extracted from the altimetric waveform are described.

(I) with the antenna pattern function (Ant) and the point distribution function (pdf):

$$W(t) = I \otimes pdf \otimes Ant \quad (1)$$

Over land surfaces, the radar waves frequently penetrate inside such medium as snow, sand or vegetation. There can be echoes from the ground and the top of vegetation, from the ground and the surface of terrestrial snow, from the surface and the snowpack layers for ice sheets. The volume part of the echo is also attenuated by the overlying transparent medium. Over continental surfaces, the echoes can be more or less specular, for example in the case of smooth and very flat surfaces, very wet surfaces or wetlands or frosted surfaces. The echo shape is also affected by the surface topography slope and curvature. In these cases, the waveform can be seen as the convolution of the 'ocean like' waveform with a 'scattering distribution' (f_{scat}) which describes the vertical profile of the reflecting surfaces:

$$W(t) = I \otimes \text{pdf} \otimes f_{\text{scat}} \otimes \text{Ant} \quad (2a)$$

The impulse response shape $I(t)$ is given by:

$$\begin{aligned} I(t) &= 0 && (t<t_0) \\ &= e^{-\delta(t-t_0)} && (t\geq t_0) \end{aligned} \quad (2b)$$

where t_0 is the time of the impact and. The specular parameter "δ" will be discussed later.

The point distribution function pdf(t) is given, assuming a Gaussian distribution, by:

$$\text{pdf}(t) = \frac{1}{s\sqrt{\pi}} e^{-\left(\frac{t-t_0}{s}\right)^2} \quad (2c)$$

where s is the rms of the surface roughness. The scattering distribution $f_{\text{scat}}(t)$ is given by:

$$\begin{aligned} f_{\text{scat}}(t) &= 0 && (t<t_0) \\ &\sigma_{\text{s}} && (t = t_0) \\ &\sigma_{\text{v}} e^{-2k_{\text{e}}c(t-t_0)} && (t_{\text{g}}>t>t_0) \\ &\sigma_{\text{g}} && (t = t_{\text{g}}) \\ &0 && (t>t_{\text{g}}) \end{aligned} \quad (2d)$$

where c is the speed of light within the medium and k_{e} the extinction coefficient, σ_{s}, σ_{v} and σ_{g} are the surface, volume and ground scattering.

In the case of surface only echoes (σ_{v}=0; σ_{g}=0) with not too much specularity the expressions reduce to the ocean-like case and the backscatter coefficient can be directly related to σ_{s} by integrating the f_{scat} function in the impulse response function. In case of more complex media, the backscatter coefficient is more difficultly related to the scattering function introduced in Eq. (2d) and needs to make the integration according to each peculiar case.

Finally, the antenna pattern function Ant is given by: $\text{Ant}(\Omega)=e^{-\alpha\Omega^2}$ where Ω is the incidence angle on the target. Which converts to:

$$\begin{aligned} Ant(t) &= 0 && (t<t_0) \\ & e^{-\left(\alpha\theta^2+\left(g_0+\beta\theta^2\right)*\gamma*(t-t_0)\right)} && (t\geq t_0) \end{aligned} \quad (2e)$$

where θ is the surface topography slope or the antenna mispointing and γ:

$$\gamma = \left(1+2Hc_{topo}\right)/(1+H/R) \quad (2f)$$

where, c_{topo} is the surface curvature, H is the satellite height and R is the earth radius. This equation takes into account the earth curvature and the surface curvature. The parameters g_0, α and β depend on the satellite orbit and antenna size (Legrésy, 1995) and we computed:

$g_0 = 4.23*10^6 s^{-1}$ for Envisat Ku band

$0.22*10^6 s^{-1}$ for Envisat S band

$\alpha = 10899\ rad^{-2}$ 3.32deg^{-2} for Envisat Ku band

$591\ rad^{-2}$ 0.18deg^{-2} for Envisat S band

$\beta = 4.497*10^{-6} s^{-1}\ rad^{-2}$ $1.37*10^7\ s^{-1}\text{deg}^{-2}$ for Envisat Ku band

$1.44*10^{-8}\ s^{-1} rad^{-2}$ $4.4*10^4 s^{-1}\text{deg}^{-2}$ for Envisat S band

Note that the surface slope affects both the whole backscattering (via α) and the trailing edge slope (via β). This dependence is far less in S band than in Ku band.

In the case of ocean and frequently soil surfaces, the surface can be assumed as an isotropic reflector so that the backscatter does not depend on the incidence angle within the typical 3° antenna aperture range of radar altimetry. The δ parameter in Eq. (2b) is then 0 and the impulse response is flat. In the case of a fully specular surface δ would be infinite. In the case of quasi-specular surfaces, the δ parameters can take a wide range of values depending on the nature of the surface. In this case, the impulse response trailing edge slope is more or less steep depending on the nature of the surface. Note that in any case, specularity can only diminish the trailing edge slope.

The different equations in Eqs. (2a)–(2f) describe most of the cases one can meet in observing the earth's natural surfaces. However, we assume the same pdf for internal layers interfaces and for the surface in case of penetration in a stratified media. We also assume that the specularity is similar for the surface and internal layers. In addition, we note that the σ_{v} and σ_{g} calculations must incorporate attenuation through the medium and interfaces.

Fig. 2 shows three examples of scattering distribution functions. In the case of ice sheet snowpack (Fig.2a), the peak at zero corresponds to the surface dielectric jump from air to snow. The exponential decrease corresponds to internal snow density jumps which create smaller echoes at each interface. These internal echoes are attenuated by the travel across the snowpack when the grains scatter the signal (Legresy & Remy, 1997). In Fig. 2b we show the scattering distribution of typical terrestrial snow areas (Papa et al., 2002). The bottom peak corresponds to the ground echo which is attenuated by the absorption and scattering while travelling across the snowpack. The peak at zero corresponds to the dielectric jump between air and the rough snow surface. In Fig. 2c we show a scattering function for the case of vegetation. The top peak corresponds to the interface between air and the top of vegetation, followed by scattered echoes by branches and/or leaves. The bottom peak corresponds to the ground echo which is attenuated by the travel across the vegetation.

2.2. Expected altimetric signal

The backscatter is controlled by the surface and the volume echoes. The surface echoes, in the case of a nadir looking angle, are controlled by the Fresnel coefficient and the surface microroughness (Fung & Eom, 1982). In some cases, depending on the scale of the roughness, the same surface may appear rough in Ku band and smooth in S band (Ulaby et al., 1982). The penetration within the medium depends on the dielectric losses (absorption and scattering) that are strongly frequency dependent. For instance, the scattering currently used in case of small scale scatterers, like snow grain, depends on the radar wavelengths to a power 4 (Fung & Eom, 1982), leading to a S band value 320 times greater than the Ku band value. Because of the antenna pattern, the backscattering is also affected by the surface slope (term α in Eq. (2e)), mostly in Ku band.

After the convolution process (Eqs. (2a)–(2f)) the leading edge width appears as an integration of the surface macroroughness and small scale topographic features and is enlarged by the penetration effects. Since S and Ku band observations are made at the same time, the surface macroroughness as perceived by each band is the same (even though electromagnetic bias processes such as the sea state bias observed on ocean surfaces might exist). Concerning the volume echo, it may infer very different values of the leading edge width, depending on the structure of the medium.

After the convolution process (Eqs. (2a)–(2f)), the trailing edge slope is enhanced by the volume effect, which signal is delayed in time. We observe a less steep trailing edge for the S band than for the Ku band. The surface specularity may also affect this part of the waveform. The trailing edge slope is also affected by surface slope and curvature (at the footprint scale, typically 10 km). In S band, the antenna aperture being rather large, we expect a trailing edge slope with little sensitivity to surface slope and curvature. In the following analysis, we often use the difference of a given altimetric parameter between the 2 frequencies which we will note C–Ku or S–Ku. . .(for example, backscatter S–Ku means the difference between S band Backscatter and Ku band Backscatter).

2.3. Principle of the altimetric waveform reprocessing

The basic altimetric data can be represented as a histogram of the energy backscattered by the ground surface, with respect to the time and is commonly called the altimetric waveform (Fig. 1). The retracker is the algorithm which tracks the point of this altimeter radar echo waveform which corresponds to the effective satellite–ground range to be measured and provides the correction to be applied to the onboard tracker estimates. This notion has been extended to include fitting the waveform with a theoretical function which describes its shape (echoing point, amplitude, leading edge width, trailing edge, asymmetry of the leading edge. . .).

The ICE-2 retracker, implemented on the ground segment of the ENVISAT RA-2 altimeter, is based on the principle of fitting the waveform shape using the Brown, 1977 model as is applied over the oceans (Brown, 1977; Dumont, 1985; Rodriguez, 1988) and over ice caps (Legresy & Remy, 1997; Martin et al., 1983). It consists in detecting the waveform edge, fitting an error function

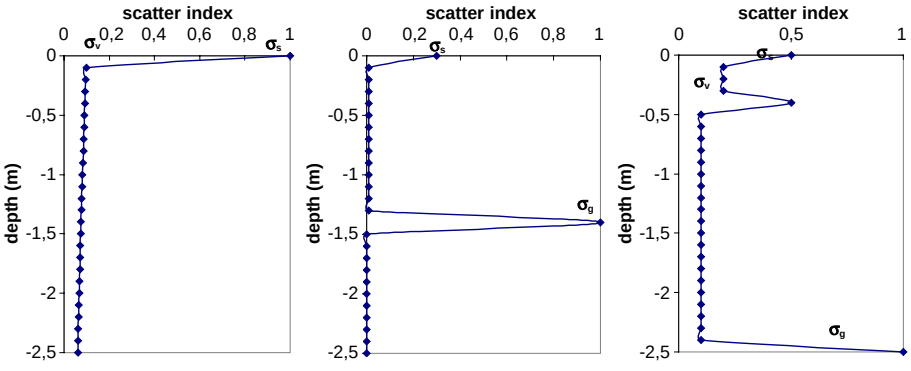

Fig. 2. Three examples of scattering distribution functions: for ice sheets snowpack (left), for terrestrial snow cover (middle) and for vegetation (right).

(erf) to the leading edge and an exponential decrease to the trailing edge (Fig. 1). The main outputs are: the Leading edge amplitude (LeBs), the Range corrected for the instrument mistracking, the Leading edge width (LeW), the trailing edge slope (TE) and the Backscatter coefficient (Bs) corresponding to the waveform integration. For the ENVISAT satellite, these parameters are provided for both the Ku and S band waveforms. The physics of the echoes over continental surfaces vary widely and often they do not correspond accurately to the model used in ICE-2. This model help describe the shape of the waveform robustly over most surfaces. In the ICE-2 retracking (Envisat product handbook; Legrésy, 1995), we assume that the trailing effects do not impact dramatically on the leading edge part of the waveform which is contrary to the oceanic devoted algorithm. This means that we can separately fit the first part to the leading edge and the second to the trailing edge of the waveform. Indeed, for continental surfaces, the trailing edge is more strongly affected by surface slope, surface curvature and volume scattering. In addition, by fitting only the first part of the waveform to the leading edge, we reduce the footprint used for the estimation of the mean topography, so we gain in spatial resolution. However, the assumption that the trailing edge variations do not impact dramatically the leading edge is not verified in the case of very specular surfaces like sea-ice or small continental water bodies. Specific retracking algorithm are needed in these cases, such as the ENVISAT sea-ice retracking (Laxon, 1994).

2.4. Envisat dataset

The RA-2 sensor onboard ENVISAT is a dual-frequency radar altimeter operating in Ku band (13.6 GHz or 2.3 cm) and S band (3.2 GHz or 9.3 cm). The dual frequency was initially designed to provide corrections for the height measurement errors due to the ionospheric delays on the signal.

ENVISAT has a 35-day repeat cycle and provides observations along its entire ground track over the ocean and continental surfaces, from 82.4° North to 82.4° South. The ENVISAT equatorial ground track spacing is about 85 km and its swath width only amounts to a few kilometres. For this study, we used data from cycles 10, 11 and 12 (October, November and December 2002) of ENVISAT which were the first ones available. These data were processed with a version of ICE-2 which was not fully validated. An edge detection problem was present in the algorithm, leading to many bad outputs (Milagro et al., 2003). This problem has since then been solved and future data will be free of this error. For this study we used a careful editing of the data removing outliers for each parameter. The main editing criteria is given by checking the LeBs difference between S and Ku band which eliminates most of the bad data and allowed us to correctly map all of the parameters. To avoid contamination of land surface data with ocean measurements, especially for locations close to the coasts, we have masked the data over the oceans. The heights have been corrected for ionosphere delay using the GIM model of Total Electron Content (http://iono.jpl.nasa.gov/index.html) since this delay applies differently to the two frequency bands. The bias in the backscatter difference between S and Ku band was estimated to be 0.5 dB over the oceans for the period considered. Other biases remain in the data, in particular for the height and backscatter coefficient. In the following analysis, we deal with relative rather than absolute values to reduce the mean bias unknown and make the lack of bias estimates clear when necessary.

For each of the parameters, we will consider an average value of the cycles 10, 11, 12 covering the period October–December 2002 which we will call Autumn 2002.

3. Altimetric signal over land

The first applications of dual frequency radar altimetry over land areas were recently started with the NRA radar altimeter on board the joint U.S.–French mission Topex–Poseidon (T–P) (Papa et al., 2003). Topex–Poseidon, has a 10-day repeat cycle and an inter-track separation at the equator of about 300 km, and operates in Ku and C bands (5.4 GHz frequency, 5.8-cm wavelength).

In Papa et al, 2003, only the altimetric backscatter coefficients in C and Ku were available and the retracking technique for processing the waveforms was only optimized for ocean surfaces. Now, ENVISAT offers for the first time the opportunities to map land surfaces using all of the altimetric parameters obtained with the ICE-2 algorithm for the Ku and S bands.

3.1. Backscattering from lands

The capabilities of using altimetric backscatters in Ku and C bands over land surfaces at regional and global scales were recently demonstrated using the 9 years span dataset of Topex–Poseidon. Papa et al. (2003) indicate the strong potential to monitor different land surface types (desert, tropical forest, savannas, boreal regions…) and their seasonal variability.

Fig. 3 shows the ENVISAT RA-2 backscatters over land in (a) Ku band, (b) S band, (c) the difference S–Ku, expressed in decibels (dB) for the autumn 2002. Fig. 3d shows the difference in backscatter C–Ku (dB) obtained for the same period with the dual-frequency radar altimeter onboard Jason-1. Jason-1 altimeter was launched in December 2001 and has the same properties as Topex–Poseidon, thus offering the opportunity to compare its observations with the ENVISAT ones over the same period.

At a global scale, the ENVISAT backscatter values range from 0 to more than 25 dB for Ku band and from a few dB to more than 35 dB in S band. This gives an overall spatial dynamic of more than 25 dB that also means a factor of

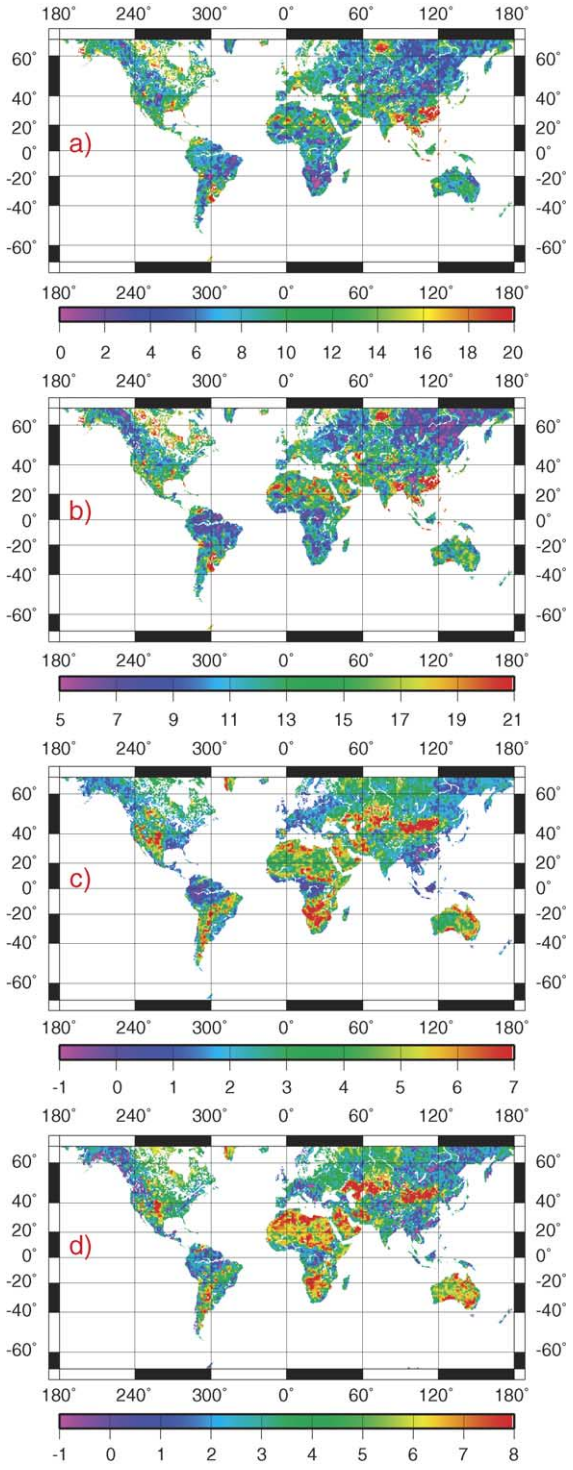

Fig. 3. Backscatter coefficient from continental surfaces for (a) ENVISAT Ku band, (b) S band, (c) S–Ku, and (d) Jason-1 C–Ku, over Autumn 2002, expressed in dB.

more than 300 in terms of power. First, these observations confirm the ones related in Papa et al. (2003) with Topex/Poseidon. For Ku and S band, the backscatter is low in mountainous regions (<7 dB in Ku band,<14 dB in S band) directly related to the presence of topographic slopes. The antenna pattern convoluted with the angle of incidence indeed decreases the return power of the altimetric echo. These responses are particularly encountered for high mountainous regions such as the Andes, the Rocky Mountains or the Himalaya. As it is observed for southern part of Africa or east part of the Brazilian coast, the backscatter can be also low for non high mountainous regions but presenting topographic slopes variations; in that case the backscatter in S band is higher because of a the larger aperture of the antenna.

For both bands, the backscatter values are high on very flat surfaces, such as deserts, large river basins or wetlands (>15 dB in Ku band and >20 dB in S band), due to the specularity of the return radar echo. This is the case for many parts of the Sahara desert, the Ob River basin or the Ganges River basin regions.

Fig. 3c shows the results for the difference in RA-2 backscatter S–Ku. It ranges from a few dB to more than 12 dB and shows a typical spectral signature of the continental surfaces: in general, high values are for arid and desert regions (>10 dB) and low values for dense tropical rain forests (<2 dB). This is in accordance with previous results from Topex–Poseidon observations. We note a close correspondence with the Jason-1 backscatter C–Ku map (Fig. 3d) over lands obtained for the autumn 2002. However, we note some differences between both maps, in particular in the central part of the Sahara desert, where RA-2 S–Ku backscatter is around 6 dB and Jason-1 C–Ku backscatter is more than 12 dB. This can be explained partly with a saturation effect on the C band in this area.

These new observations bring new advantages to use RA-2 backscatter in S band over lands with an extension of the range of scattering medium observable (like vegetation density for example).

3.2. Leading edge width over lands

Fig. 4 shows, at the global scale, the leading edge width, namely LeW (m) over lands in Ku band (Fig. 4a), in S band (Fig. 4b) and the difference S–Ku (Fig. 4c) obtained with RA-2 for the period autumn 2002.

According to the theory, the leading edge width is related to the penetration into the medium and the surface roughness of the target (Legresy & Remy, 1998). We note large variations in space of more than 2 m for the Ku band and more than 3 m for the S band. The leading edge width values are high in desert areas (see for instance the Sahara or the Takla Makan) due to the strong penetration of the wave and the dunes generated by the winds. The low values, related to a weak penetration are for dense vegetated areas, such as tropical or boreal forests, or for large river basin or inundated regions. In contrast to the backscatter coefficient, the use of only one frequency gives a typical signature of the continental surfaces, providing a good discrimination of forests, deserts....

The leading edge width difference S–Ku has a spatial variations of more than 1 m. The difference S–Ku is low on

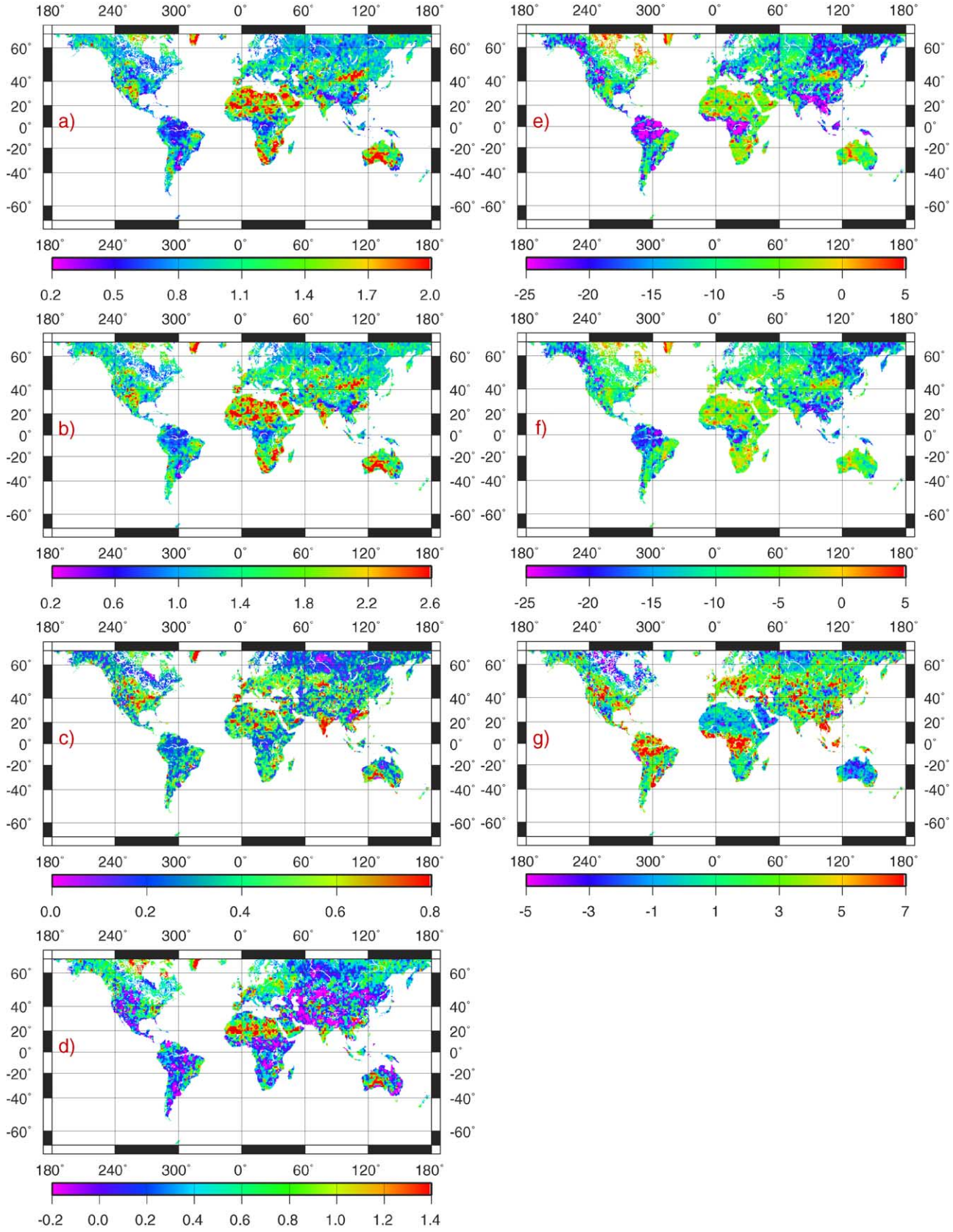

Fig. 4. Leading edge width LeW over continental surfaces for (a) Ku band, (b) S band, (c) S–Ku, expressed in m. The difference in height between both frequencies, expressed in m, is also shown (d). The trailing edge slope over continental surfaces for (e) Ku band, (f) S band, (g) S–Ku, expressed in 10^6 s^{-1}.

dense tropical or boreal forests (<0.2 m). The highest values are over India and South East Asia (>1m). For these regions the difference in backscatter S–Ku (Fig. 3c) is low (<4 dB) suggesting a penetrating and scattering medium.

Fig. 4d shows the difference in altimetric height Ku–S (m) for Autumn 2002. This map needs to be interpreted with care since this parameter has an unrecovered bias in the range between the S and Ku band measurements. However, we note a close correspondence with the difference in leading edge width S–Ku (m) which reinforces the hypothesis that it represents a penetration effect.

3.3. Trailing edge over lands

Fig. 4 shows the trailing edge slope (10^6 s^{-1}) at the global scale over lands, in Ku (Fig. 4e), S (Fig. 4f) and S–Ku (Fig. 4g) for autumn 2002.

The trailing edge slope is related to the echo specularity, the penetration into the medium and the slope effects. The Trailing Edge Slope in S band is naturally higher than in Ku band due to the difference in antenna aperture. Over ocean surfaces, the mean value of the trailing edge slope is $-3.76*10^6$ s^{-1} in Ku band and $-0.196*10^6$ s^{-1} in S band so the 'natural difference' between both is around $3.5*10^6$ s^{-1}.

In Ku band, low values are for the tropical dense forests ($<-30*10^6$ s^{-1}) and vegetated areas of Europe confirming the low penetration into this medium and specular reflection at the top of the forest canopy. For the same areas, the trailing edge in S is also low, showing the same behaviour as Ku. Over the Northern East part of Canada, the Ku band trailing edge rise ($>5*10^6$ s^{-1}) and even higher than for the S band (around $-3*10^6$ s^{-1}). The difference in trailing edge is significantly negative and confirms the fact that at the beginning of winter, the Ku band is more sensitive to thin snow cover than S band is (as observed with Ku and C band by Papa et al., 2002).

Over deserts and sparsely vegetated areas, the S and Ku band trailing edge slope rise due to slope and penetration effects, and the S–Ku increases above the 'natural difference' value due to the stronger penetration in the S band.

4. Altimetric signal over ice caps

While ENVISAT gives more spatial resolution compared to Topex–Poseidon and Jason, it also extends the dual frequency observations higher into the polar regions, up to 81.4° latitude. This means we can observe 80% of the Antarctic ice cap and quite 100% of the Greenland ice cap.

We have mapped each parameter over Antarctica (left side of Figs. 5, 6 and 7) and Greenland (right side of Figs. 5, 6 and 7) ice caps. The maps in Ku band have already been produced using ERS altimeter data (Legresy & Remy, 1997). ENVISAT allows us to map the parameters in S Band and the difference between S and Ku band for each parameter.

4.1. Backscattering from ice caps

The backscatter (Fig. 5) is low over low altitude areas, for both ice sheets, due to the high surface slope near the coast (see Eq. (2e)). In Ku band, it is also low in these lower altitude regions of the East Antarctic ice cap because the katabatic winds flow intensively and carve the surface making it very rough at the centimetre scale. Higher snow accumulation rates in these low altitude regions participate in increasing the surface roughness (Bromwich et al., 1990). At high altitude, the backscatter increases as the wind and the surface roughness decrease. In Droning Maud Land (near 0° longitude) as well as in the western part of the West Antarctic ice cap very high backscatter areas reveal a very smooth surface, this may result from a snow accumulation anomaly produced by the wind induced snow transport (Legresy & Remy, 1998). Over Greenland the same analysis applies, but the wind is less strong than in Antarctica and melting occurs on coastal areas. In particular, all the way around the Greenland, the melting/refreezing produces a specular reflection of the radar waves on steep slopes. When the surface is sloping, the impact point is shifted in the upslope direction and do not coincide with the nadir. When these slopes are greater than the altimeter antenna aperture, as it is the case near the ice sheet coast, the energy received by the altimeter is very low. At higher altitude and latitude, the accumulation rates decrease along with the surface centimetre scale roughness so higher backscatter coefficients are then observed.

In the S band, the radar waves penetrate deeper in the snowpack than in the Ku band and since the antenna aperture is larger, it is less sensitive to the slope effect than for the Ku band (Eq. (2e)). Over Antarctica, the pattern of the backscatter is similar to that of the Ku band and a similar analysis is valid. Over Greenland, the S band pattern is similar to the Ku one, except that the margins have a higher backscatter coefficient since the antenna can catch the main return signal from the more moderate slopes. In the south-western part we can observe a band of very high backscatter which was not present on the Ku band map. It corresponds to a large percolation zone where melting occurs in summer. Since S band waves penetrate deeper in the snowpack, internal icy layers are thus better seen using this radar frequency and participate much more to the average return.

The backscatter difference between the S and Ku bands reveals the differences in the echoing physics. Over East Antarctica, the high altitude low accumulation area is very stratified and since the S band waves are less attenuated by the snow grain, they are better reflected from the internal strata providing a bigger total return than for the Ku. In contrast, over the windy and snow depositional areas, the S band integrates less surface signal and the deep penetration of the waves allows the signal to be scattered giving a lower total return than for the Ku band. Over Greenland, over the north areas where both altitude and latitude are high, the snow accumulation rate is weak so that the difference in

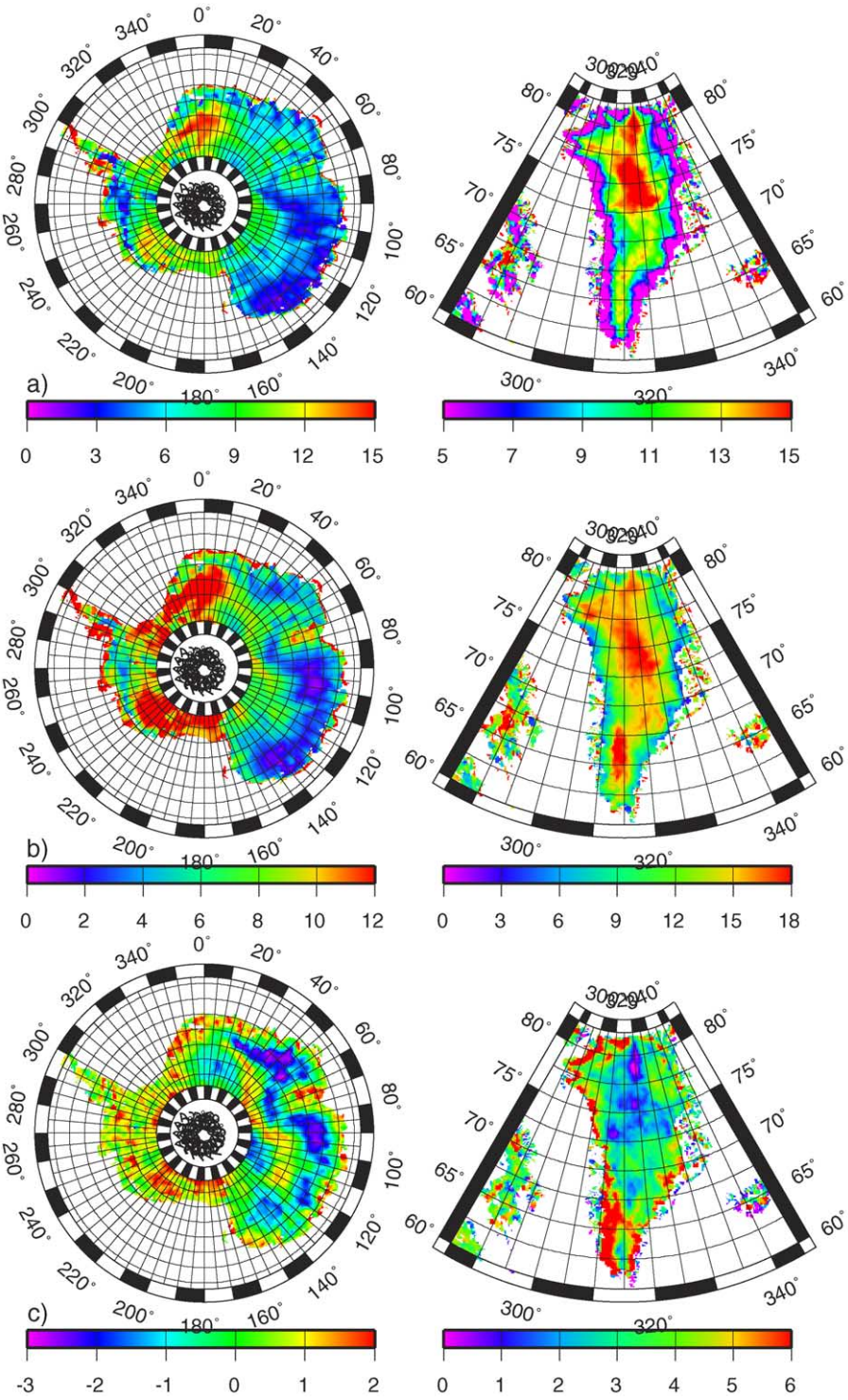

Fig. 5. Backscatter coefficient from Antarctica (left panel) and Greenland (right panel) for (a) Ku band, (b) S band, (c) S–Ku, expressed in dB.

backscattering is quite small. On the contrary, the percolation zone in south Greenland (Benson, 1962) is clearly revealed. Note that a very different scale of up to more than 6 dB difference is necessary to map this signal, clearly revealing that the percolation zone makes the very essential difference between the Antarctic and the Greenland backscatter physics.

4.2. Leading edge width over ice caps

In the Ku band over Antarctica and over Greenland (Fig. 6), we find essentially the same map as for ERS. The leading edge width LeW has small values inland at high altitude low accumulation, low roughness areas with increasing values toward the coast where there is increasing roughness and

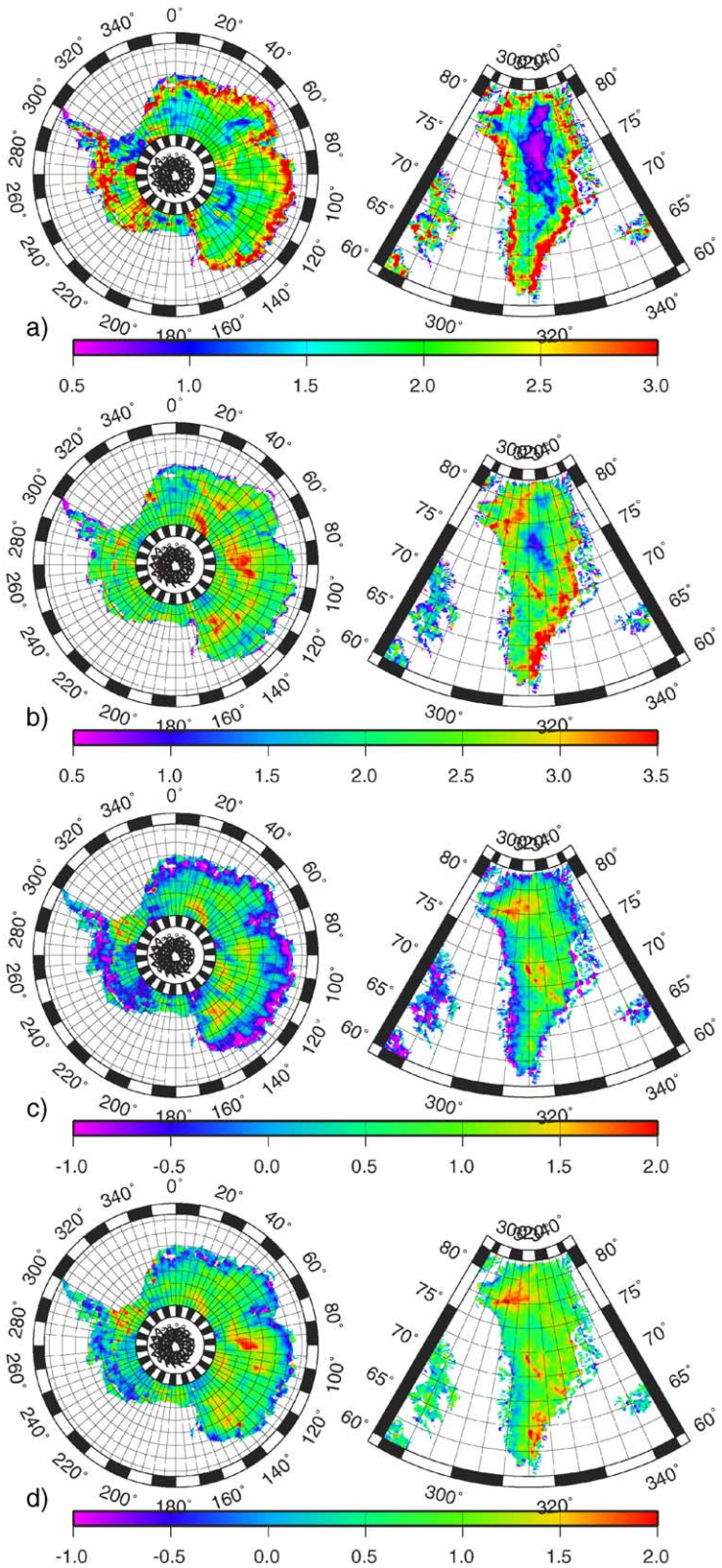

Fig. 6. Leading edge width LeW over Antarctica (left panel) and Greenland (right panel) for (a) Ku band, (b) S band, (c) S–Ku, expressed in m. The difference in height between both frequencies, expressed in m, is also shown (d).

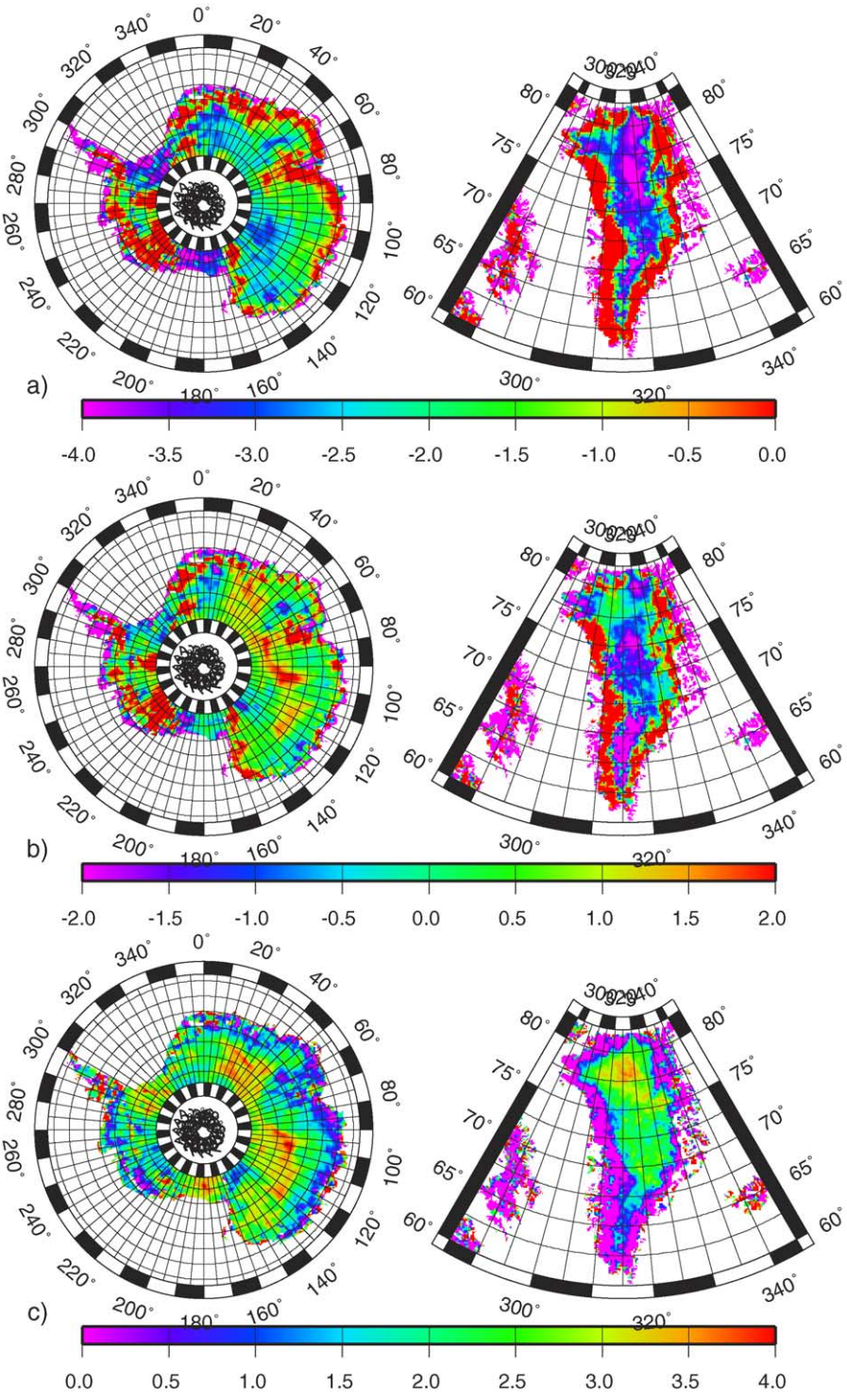

Fig. 7. Trailing edge slope over Antarctica (left panel) and Greenland (right panel) for (a) Ku band, (b) S band, (c) S–Ku, expressed in 106 s−1.

volume echo. In the S band, the picture is quite different over Antarctica, the S band has greater values than the Ku band on the plateau, tending to be smaller toward the coastal area. The map of the difference of leading edge width between both bands clearly reveals this unexpected signal. This difference is less obvious over Greenland where the difference between both leading edge widths never reaches negative values.

In order to explain these rather small values of leading edge width we have mapped the height difference Ku–S. This difference may either indicate a difference in one of the delay errors which applies differently to both frequencies (mainly the ionosphere and surface state bias corrections which are frequency dependant) or a difference in the volume echo between both frequencies, which reveals the

difference in penetration depth between the two frequencies. Note that a difference in the electromagnetic bias would lead to the S band height being less than the Ku band height with a narrower leading edge in the S band.

We find a fairly good correlation between the leading edge width difference and the height difference (0.77) with a regression factor of 1, meaning that half of the height difference can be explained by the leading edge width difference. In general lower frequencies penetrate deeper into the snowpack and the difference between the measured Ku and S band height must be positive, as is observed for Greenland. In contrast, in the marginal regions, around Antarctica (150 km from the coast), the Ku band height is found below the S band and the Ku band leading edge is found smaller than the S band one.

If there was no penetration in any of the two bands, they should measure the same height. If penetration occurs in a transparent medium, the S band should penetrate deeper. However, the surface centimetre scale roughness may be seen differently by the Ku and S bands. If so, the S band surface backscatter might be larger and a larger quantity of the reflected signal coming back from inside the snowpack might be reflected down by the surface air–snow interface. Then the S band waveforms may be controlled by a surface echo with a marginal volume echo. In this case, the leading edge width would reflect only the surface metre to hectometre scale roughness height. The Ku band would include the sum of the delayed internal echoes and have an enlarged leading edge. This particular behaviour of altimetric echoing over ice caps is a new observation which has been revealed by this ENVISAT dataset and needs to be further investigated in dedicated studies.

4.3. Trailing edge slope

Fig. 7 shows maps of the trailing edge slope in both Ku and S band and their difference over Antarctica and Greenland. The penetration depth in Ku band has been previously estimated by Legresy and Remy (1998): it is a few metres in the central part of the Antarctica and increases toward the coast (Legresy & Remy, 1998). The impact on the trailing edge tends to add to the slope effect which in turn increases the trailing edge slope toward the coast. In regions where the backscatter is high, for example high in the interior of Droning Maud Land or near (140° E; 80° S), the surface topography is very smooth, the accumulation rates are small and the snowpack is very stratified. Here, the echo is more specular and we find very low trailing edge slopes. In the northern plateau of the Greenland ice sheet, we find a similar situation, with even more specular echoes.

In the S band over Antarctica, the trailing edge slope increases toward the interior regions. Indeed, in this band this parameter is less affected by the surface slope and mostly controlled by volume echo. The difference between both trailing edge slopes reveals the difference in the penetration between both frequencies. Indeed, this map (Fig. 5c) is very similar to the penetration depth in the Ku band already mapped over Antarctica by Legresy and Remy (1998).

For Greenland, the situation is slightly different. Although the large scale pattern of the trailing edge is quite similar for both frequencies and follows the slope effects, the difference S–Ku increases toward the interior as for Antarctica.

5. Discussion and conclusion

In summary, ENVISAT measurements from the ICE-2 processing chain offers from now a complete dual-frequency radar altimeter dataset devoted to any types of surface from lands to ice sheets up to 81.4° latitude.

First, the ENVISAT observations offer continuity to the Earth survey with radar altimeter started at the beginning of the 1990s. The first results from the Ku bands are in accordance with the previous ERS data processed over ice sheets (Legresy & Remy, 1997). Over lands, the ENVISAT measurements are also similar to results obtained from inland altimetry using Topex–Poseidon Ku band measurements (Papa et al, 2003). Moreover, the ENVISAT measurements are editing with more confidence as these data are processed and devoted to continental applications. For instance, as described for Topex–Poseidon radar altimeter in Papa et al., 2002, ENVISAT Ku band data can be used to survey terrestrial snowpack evolution to determine important climatic parameters such as the beginning and the end of the snow season or the snow depth evolution. With Topex–Poseidon, only the backscatter was available whereas ENVISAT offers all the waveform parameters that will help to better understand the signals such as surface roughness and penetration contributions and give more accurate estimations. Advantage of ENVISAT in that context is also a better spatial resolution for local studies.

The results with ENVISAT altimeter observations also reinforce the new potentials of the use of dual-frequency measurements over continental surfaces. The use of dual-frequency radar altimeter backscattering coefficients starts recently with Topex–Poseidon observations. The ENVISAT S band measurements are first in accordance with expected observations from theory as well as, they also confirm the previous C band Topex–Poseidon backscatter observations over land (Papa et al, 2003). In that context, the S band observations drastically offer new potentials to survey land surfaces. For instance, using the Topex–Poseidon C band backscatter signal, it seems possible to retrieve wetlands extend and their seasonal variability. The dual-frequency observations are in that context useful to determine the vegetation contribution to the altimetric signal. The ENVISAT waveform parameters in S band lead to a new way to better quantify this contribution and to make more accurate estimation of flooded areas including those that are densely vegetated areas.

Moreover, because Topex–Poseidon observations were limited to 66° latitude, ENVISAT radar altimeter gives the first dual-frequency observations over ice caps surfaces opening new perspectives. For instance, within the temporal survey of ice sheets surface topography with radar altimeter, the penetration of the wave within the snowpack strongly affects the height estimation as seen by the satellite. An induced error due to change in snowpack may then affect the interpretation of altimetric series. Because the penetration mostly depends on the volume scattering that depends on the radar frequency, dual-frequency altimeter allows detecting and estimating this penetration error giving a better accuracy on the heights measurements. Moreover, using the same properties of frequency and volume scattering dependence, the dual-frequency radar altimeter over ice sheets will also help to retrieve important parameters such as the snowpack characteristics.

In conclusion, this first study with these new data shows the physical characteristics of the altimeter measurements and as we see opens a large range of potential applications. Further studies should concentrate on particular phenomena and bring more quantitative results. Inverse modelling as such already performed by Legresy and Remy (1998) over Antarctica will be a key tool to attain such goals.

The combination of ENVISAT data with Topex/Poseidon and Jason-1 data will give a unique tri-frequency observation at vertical incidence to better describe and survey the continental surfaces. The time variations of these measurements also promise an efficient survey of the evolution of many continental surface processes.

Finally, using these parameters to understand the nature of radar altimeter echoes will help to improve the interpretation and survey of the height measurements which become more confident over land with the dual-frequency robust tracking radar altimeter of ENVISAT.

Acknowledgements

This paper is a contribution to the Validation of the ESA ENVISAT RA-2. This work is part of the OSCAR project; all data grids presented here will be placed on the LEGOS website freely available after publication of the paper. It benefited from useful discussion with Patrick Vincent from CNES and from a very useful review of Rosemary Morrow from LEGOS/CTOH who made the English Language much better written. It also benefited from the constructive comments of 3 anonymous reviewers.

References

Alsdorf, D., Birkett, C., Dunne, T., Melack, J., & Hess, L. (2001). Water level changes in Large Amazon Lake measured with spaceborn radar interferometry and altimetry. *Geophysical Research Letter*, *28*(14), 2671–2674.

Benson, C. S. (1962). Stratigraphic Studies in the Snow and Firn of the Greenland Ice Sheet. U.S. Arm. SIPRE Report. 70.

Birkett, C. M. (1995). The contribution of Topex/Poseidon to the global monitoring of climatically sensitive lakes. *Journal of Geophysical Research*, *100*(C12), 25179–25204.

Bromwich, D. H., Parish, T. R., & Zorman, C. A. (1990). The confluence zone of the intense katabatic winds at Terra Nova Bay, Antarctica, as derived from airborne sastrugi surveys and mesoscale numerical modelling. *Journal of Geophysical Research*, *95*(D5), 5495–5509.

Brown, G. S. (1977). The average impulse response of a rough surface and its application. *IEEE Transactions on Antennas and Propagation AP*, *25*, 67–73.

Cazenave, A., Bonnefond, P., & DoMinh, K. (1997). Caspian sea level from Topex/Poseidon altimetry: Level now falling. *Geophysical Research Letter*, *24*(8), 881–884.

Dumont, J. P. (1985). Estimation optimale des parameters altimetriques. PhD thesis INPT Toulouse, France.

Envisat RA2/MWR Product Handbook PO-TN-ESR-RA-0050 Issue 1.2 22/03/2002 http://envisat.esa.int/dataproducts/ra2-mwr

Fu, L. L., & Cazenave, A. (2001). Satellite Altimetry and Earth Science, A Handbook of Techniques and Applications. London (UK): Academic Press.

Fung, A. K., & Eom, H. J. (1982). Application of a combined rough surface and volume scattering theory to sea ice and snow backscatter. *IEEE Transactions on Geoscience and Remote Sensing*, *GE-20*, 4528–4536.

Laxon, S. (1994). Sea ice altimeter processing scheme at the EODC. *International Journal of Remote Sensing*, *15*(4), 915–924.

Legrésy, B. (1995). Etude du retracking des formes d'onde altimétriques au-dessus des calottes polaires. CNES report CT/ED/TU/UD/96.188 contract no. 856/2/95/CNES/006.

Legresy, B., & Remy, F. (1997). Surface characteristics of the Antarctic ice sheet and altimetric observations. *Journal of Glaciology*, *43*(144), 265–275.

Legresy, B., & Remy, F. (1998). Using the temporal variability of the radar altimetric signal to map surface characteristics of the Antarctic ice sheet. *Journal of Glaciology*, *44*(147), 197–206.

Martin, T. V., Zwally, H. J., Brenner, A. C., & Bindschadler, R. A. (1983). Analysis and retracking of continental ice sheet radar altimeter waveforms. *Journal of Geophysical Research*, *88*, 1608–1616.

Milagro, M., Soussi, B., Baker, S., Zanife, O. Z., Dumont, J. P., Muir, A., et al. (2003). Verification of the RA2/MWR level 2 geophysical refence processors. Proc. Of the Envisat Validation Workshop. ESRIN Frascati.

Papa, F., Legresy, B., Mognard, N. M., Josberger, E. G., & Remy, F. (2002). Estimating terrestrial snow depth with the Topex–Poseidon altimeter and radiometer. *IEEE Transactions on Geoscience and Remote Sensing*, *40*(10), 2162–2169.

Papa, F., Legresy, B., & Remy, F. (2003). Use of the Topex–Poseidon dual-frequency radar altimeter over land surfaces. *Remote Sensing of Environment*, *87*, 136–147.

Remy, F., Brossier, C., & Minster, J. F. (1990). Intensity of a radar altimeter over continental ice sheets. A potential measurement of surface roughness and katabatic wind intensity. *Journal of Glaciology*, *36*, 133–142.

Remy, F., Legresy, B., Bleuzen, S., Vincent, P., & Minster, J. F. (1996). Dual-frequency Topex altimeter observation of Greenland. *Journal of Electron Waves and Aplliance*, *10*, 1505–1523.

Remy, F., Schaeffer, P., & Legresy, B. (1999). Ice flow physical processes derived from ERS-1 high resolution map of the Antarctica and the Greenland ice sheets. *International Journal of Geophysics*, *139*, 645–649.

Rodriguez, E. (1988). Altimetry for non-Gaussian Oceans: Height biases and estimation of parameters. *Journal of Geophysical Research*, *93*, 14107–14120.

Ulaby, F. T., Moore, R. K., & Fung, A. K. (1982). Microwave remote sensing: Active and passive. *Radar Remote Sensing and Surface Scattering and Emission*, *vol. II*. Artech House, Norwood (USA): Addison-Wesley Publishing.

Vinay, G., Pace, O., Legresy, B., Remy, F. (2002). Global survey of the earth surfaces with ERS radar altimetry. EGS02-A-03704 Geophys. Res. Abs. Vol. 4.

Zwally, H. J., Bindschader, R. A., Brenner, A. C., Martin, T. V., & Thomas, R. H. (1983). Surface elevation contours of Greenland and Antarctica ice sheets. *Journal of Geophysical Research*, *88*, 1589–1596.

Zwally, H. J., Brenner, A. C., Major, J. A., Bindscadler, R. A., & Marsh, J. (1989). Growth of Greenland ice sheet: Measurement. *Science*, *246*, 1587–1589.